PROCEEDINGS OF SCIENCE

Feasibility study on an analysis of CR helium flux with the CALET detector based on an extended acceptance

M.Mattiazzi[a,b,*] **and P.Brogi**[a,c] **for the CALET collaboration**

[a] *Department of Physical Sciences, Earth and Environment, University of Siena, via Roma 56, 53100 Siena, Italy*

[b] *INFN Sezione di Padova, Via Marzolo, 8, 35131 Padova, Italy*

[c] *INFN Sezione di Pisa, Polo Fibonacci, Largo B. Pontecorvo, 3, 56127 Pisa, Italy*

E-mail: m.mattiazzi@student.unisi.it

In this work, we present a feasibility study aiming at a measurement of the cosmic ray (CR) helium flux utilizing CALET data with a significantly enhanced statistical precision. It is based on a wider geometrical acceptance compared to the current CALET analysis while ensuring a correct identification of charged particles crossing the detector. The expected statistical enhancement for the all-acceptance configuration is nearly a factor of two compared to the previous analysis, over the entire energy range from tens of GeV to hundreds of TeV. Preliminary assessment of efficiencies and background sources has been carried out based on energy-dependent charge selections.

38th International Cosmic Ray Conference (ICRC2023)
26 July - 3 August, 2023
Nagoya, Japan

*Speaker

PoS(ICRC2023)082

1. Introduction

The CALorimetric Electron Telescope (CALET) is a space-based experiment operating on-board the International Space Station (ISS) since August 2015 and taking data smoothly since mid-October 2015. It is composed of three sub-systems for cosmic ray detection. At the top of the instrument is the CHarge Detector (CHD), a two-layer hodoscope segmented into 14 plastic scintillator paddles, with dimensions 32 mm (W) $\times$ 10 mm (H) $\times$ 450 mm (L). The two arrays of paddles are oriented perpendicularly, providing an independent charge measurement of the incoming particle for each view. Beneath the CHD is the calorimeter with a total thickness of 30 X_0, which is in turn divided into two sub-detectors. The upper sub-detector consists of the IMaging Calorimeter (IMC), a fine-grained pre-shower sampling calorimeter with a thickness of 3 X_0, enabling independent charge assessment through multiple dE/dx samplings. It consists of 7 layers of tungsten plates, each separated by two alternate layers of square scintillating fibers with cross section 1 mm^2 and length 448 mm. The particle showers are sampled every 0.2 X_0 by the first 5 layers, whereas the last two layers provide 1.0 X_0 sampling. Below the IMC is the Total AbSorption Calorimeter (TASC), a homogeneous calorimeter with a thickness of 27 X_0. It consists of 12 layers, each composed of an array of 16 lead-tungstate (PWO) logs with dimensions 19 mm (W) $\times$ 20 mm (H) $\times$ 450 mm (L). These are aligned in pairs along the directions x - y and permit the reconstruction of the shower profile, discriminating between electromagnetic and hadronic showers with high rejection power.

The helium flux measurement with CALET has been recently published [3], covering a wide energy range from $\sim$ 40 GeV to $\sim$ 250 TeV. The measured spectrum confirms the deviation of the flux from a single power law, with a progressive spectral hardening from a few hundred GeV to a few tens of TeV and the onset of a softening around 30 TeV. At higher energies, the largest source of uncertainty is due to the limited number of events. In this work we present a feasibility study aiming at an enhanced statistical precision for the CR helium flux measurement with CALET data at high energies. It is based on a wider acceptance with respect to the present fiducial acceptance $\mathbf{A_1}$ defined in [3] while ensuring a correct identification of helium nuclei crossing the detector.

2. Acceptance categories

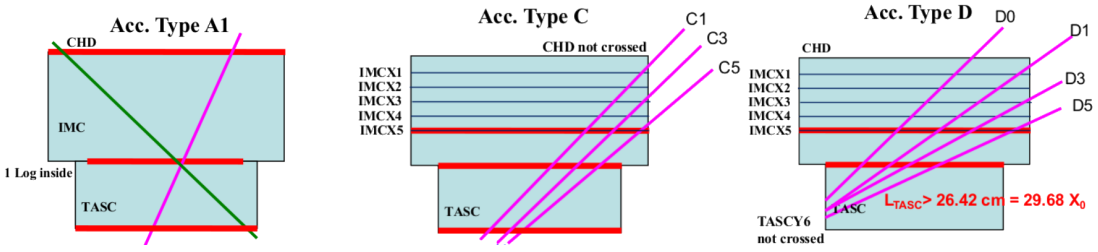

Figure 1: Definition of geometric configurations. Type A_1 is used in current helium analysis [3].

The acceptance $\mathbf{A_1}$ and the additional geometric configurations studied in this work are illustrated in Fig. 1. In detail, for $\mathbf{A_1}$, the reconstructed track must cross the entire detector, from the top of the CHD to the bottom of the TASC, with a 2 cm margin from the edge of the TASC first layer.

For $\mathbf{C_i}$, the track must cross the entire TASC and the IMC starting from the i-th layer. For $\mathbf{D_i}$, the track must traverse the IMC detector starting from the i-th layer and at least 27 cm (equivalent to $\sim 30X_0$) of the TASC to ensure a reliable energy determination. For geometry $\mathbf{D_0}$, the incoming particle must also cross the entire CHD.

3. Selection criteria

3.1 Pre-selection

The first step of the analysis procedure is based on a set of common criteria for selecting a well-reconstructed sample of events, both for the $\mathbf{A_1}$ and the other geometric configurations. Such event selections are optimized using Monte Carlo (MC) simulations based on the EPICS simulation package [7], which makes it possible to reproduce both the detector configuration and the detector response based on the physical processes involved. The pre-selection is realized by applying the following cuts :

Off-line trigger validation relies on more stringent thresholds than the on-line trigger for handling variations of detector gains.

Track quality cut ensures a high-quality track selection using performance metrics derived from the application of the combinatorial KF tracking algorithm [1].

Geometric requirements classify the reconstructed track based on the fiducial volume traversed, as defined above.

Electron rejection cut is based on an empirical Moliere concentration and on the fraction of energy deposited in the last layer of the TASC.

More details about the data analysis can be found in Refs. [2, 3].

3.2 Off-acceptance background rejection based on Boosted Decision Trees (BDT)

In the track reconstruction, it may occasionally occur that a secondary is mislabeled as a primary particle. Such events are classified as off-acceptance background and, for acceptance $\mathbf{A_1}$, they are rejected with high-efficiency by the set of cuts described in [3]. Instead, for the other geometrical conditions, a progressive enhancement of the off-acceptance background is observed as the inclination of the track increases. This is mainly due to the partial degradation of the tracking performance, resulting from the limited shower development in the TASC for high tilt angle events. Just by acceptance $\mathbf{C_1 + D_1}$, off-acceptance background grows to more than double comparing to the same component in acceptance $\mathbf{A_1}$, as can be seen in Fig. 2.

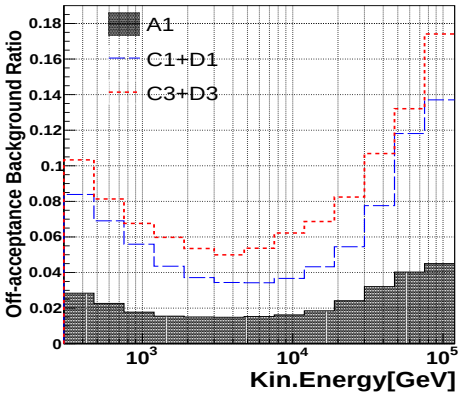

Figure 2: Off-acceptance background component for acceptances $\mathbf{A_1}$, $\mathbf{C_1 + D_1}$ and $\mathbf{C_3 + D_3}$ applying standard selections.

A machine learning approach, based on Boosted Decision Trees (BDT), has been tested, aiming to improve the rejection of such background. This

has the benefit that the selections rely on the topology of the reconstructed event. As a result of preliminary studies based on the comparison between flight data (FD) and Monte Carlo simulated distributions, the variables showing the best signal-to-background separation have been considered. The selected input features are:

- Energy deposition profile, based on the fraction of energy deposited on each TASC layer. All layers, except the 2^{nd} ,3^{rd} and 4^{th} , have been used.
- Topological variables built from the difference between the track reconstructed with combinatorial Kalman filter and with the method of moments [4]. The former mainly exploits the information provided by the IMC sub-system, whereas the latter leverages on the TASC segmentation. In detail, Δ^X_{TK} (Δ^Y_{TK}), defined as the difference between the positions in X (Y) coordinates of the impact point on the first TASC layer, and Θ^X_{TK} (Θ^Y_{TK}), defined as the difference between the reconstructed angles of the tracks in X (Y) views, have been selected.

Next, BDT classifiers have been evaluated in 6 large bins of deposited energy[1] for the configurations $\mathbf{A_1 + D_0}$, $\mathbf{C_1 + D_1}$, $\mathbf{C_2 + D_2}$ and $\mathbf{C_3 + D_3}$. The reliability of the BDT model has been assessed by randomly dividing MC data into training and test samples to check the agreement of signal and background classifier distributions. To set the BDT working point, the maximum of significance has been estimated for each energy bin. Some results for the energy bin 6.5 TeV $< E^{TASC}_{dep} <$ 20 TeV are illustrated in Fig. 3.

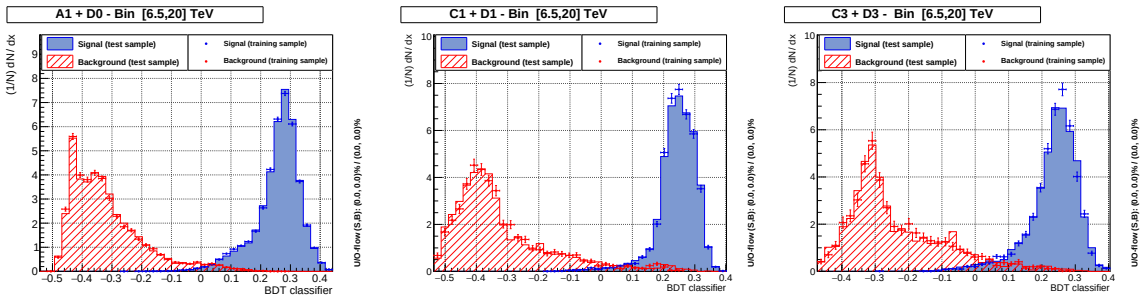

Figure 3: BDT model performance evaluated splitting randomly the MC data in test and training samples, for the configurations $\mathbf{A_1 + D_0}$, $\mathbf{C_1 + D_1}$ and $\mathbf{C_3 + D_3}$ in the energy bin 6.5 TeV $< E^{TASC}_{dep} <$ 20 TeV. The BDT classifier distributions of the test samples are represented by histograms filled in blue (signal) and red (background) respectively. The same distributions from the training samples are superimposed with markers.

3.3 Charge identification

Charge identification is of paramount importance in the helium analysis in order to achieve reliable proton rejection over the entire energy range. As shown in Fig. 4, the helium charge distributions become broader with increasing energy and track tilt. Therefore, energy-dependent charge selections have been carried out for each combined acceptance, with a procedure analogous to that applied in [3].

[1] In detail, the `TMVA` package [5] has been used. The E^{TASC}_{dep} energy intervals are: $<$ 30 GeV, 30 – 120 GeV, 120 – 300 GeV, 300 GeV –6.5 TeV, 6.5 – 20 TeV, $>$ 20 TeV.

Proton and helium charge distributions from FD and MC samples are fitted with the convolution of a Landau with a Gaussian distribution (*Langaus*). Peak position μ , the LHWHM σ_L and the RHWHM σ_R, defined as $\sigma_R + \sigma_L$ = FWHM, are extracted for each energy bin. Then, the same quantities are interpolated with high-order logarithmic polynomials[2] such that they are continuously defined for each energy deposited. For this analysis, helium events are selected according to

$$\mu_{\mathrm{He}}(\mathrm{E}) - \mathrm{n_L}\sigma_{\mathrm{L}}(\mathrm{E}) \; < \; \mathrm{Z} \; < \; \mu_{\mathrm{He}}(\mathrm{E}) + \mathrm{n_R}\sigma_{\mathrm{R}}(\mathrm{E})$$

where $\mathrm{n_R}$ is fixed at 5 over the entire energy range, whereas $\mathrm{n_L}$ is initially set to 3 and then it is lowered to 2 in the region of higher energies, taking into account the broadening of the charge distribution with respect to the number of IMC layers crossed by the track (related to the track tilt angle), as shown in Fig. 4. This approach allows a nearly flat charge selection efficiency above 500 GeV, while containing the rise of proton contamination.

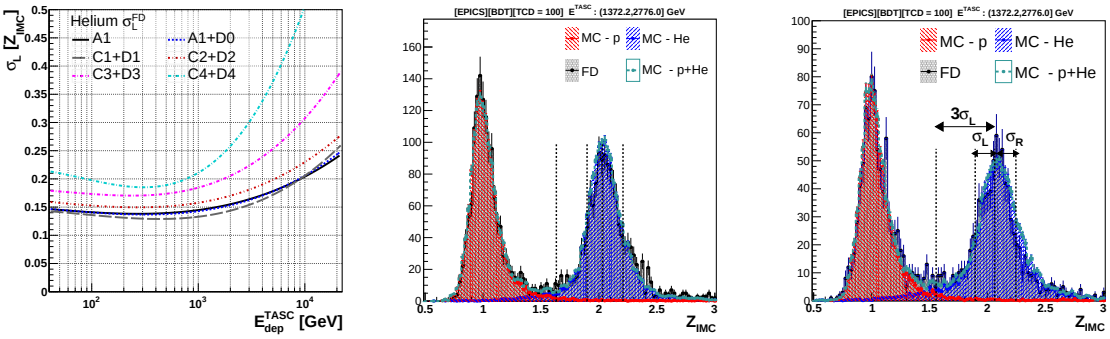

Figure 4: (Left) σ_L for FD as function of TASC deposited energy for acceptances $\mathbf{A_1}$, $\mathbf{A_1 + D_0}$, and $\mathbf{C_i + D_i}$. (Right) Charge distributions for acceptances $\mathbf{C_1}$+$\mathbf{D_1}$and $\mathbf{C_2}$+$\mathbf{D_2}$ in the energy bin 1.4 TeV $< \mathrm{E}_{\mathrm{dep}}^{\mathrm{TASC}} <$ 2.8 TeV. The distributions from MC proton and helium samples are superimposed to FD. The dashed vertical lines represent respectively, from left to right, the lower bound of the charge selection at $3\sigma_L$, the σ_L and σ_R from the *Langaus* fit.

Further extensions to highly tilted events, acceptances $\mathbf{C_4 + D_4}$ and $\mathbf{C_5 + D_5}$, require additional work and are not included in this paper.

Table 1: Geometric factors and the related statistical gain for $\mathbf{K_1}$ and $\mathbf{K_3}$ extended acceptance types.

Acceptance Type	Geometric Factor [cm^2 sr]	Statistical Gain (normalized to $\mathrm{A_1}$)
$\mathbf{A_1}$	510	1
$\mathbf{K_1}$= $\mathrm{A_1 + D_0 + (C_1 + D_1)}$	688	1.35
$\mathbf{K_3}$ = $\mathrm{K_2 + (C_3 + D_3)}$	819.6	1.6

4. Feasibility studies on extended acceptance configurations

The extended acceptances $\mathbf{K_m} = \mathrm{A_1 + D_0 + \sum_{i=1}^{m}(C_i + D_i)}$ have been defined where only the IMC sub-system is used for charge identification. The statistical gain that can be estimated from

[2]Defined as $p_n(E) = \sum_{i=0}^{n} c_i \log(E)^i$. A third order log-polynomial was chosen for this analysis.

the geometrical factor is summarized in Table 1.

4.1 Energy range

The energy range over which the extended acceptance is beneficial has been estimated by computing a purity estimator. This is evaluated bin-by-bin as the ratio of the expected number of helium nuclei after the background[3] subtraction (signal), divided by the total number of events reconstructed as helium (signal + background). As shown in Fig. 5, the purity analysis indicates that comparable or even better performances are achieved above nearly 2 TeV. Between about 500 GeV and 2 TeV, the purity in acceptance $\mathbf{A_1}$ is slightly better than $\mathbf{K_3}$. Nevertheless, the level of purity for $\mathbf{K_3}$ remains above 90%. Thus, it seems reasonable to adopt the proposed extended acceptance above 500 GeV in kinetic energy.

The improved performance at high energies can be attributed to the new BDT-based analysis strategy. In contrast, the worse performance at low energies is due to the absence of the CHD sub-system for charge identification, resulting in an increased proton contamination.

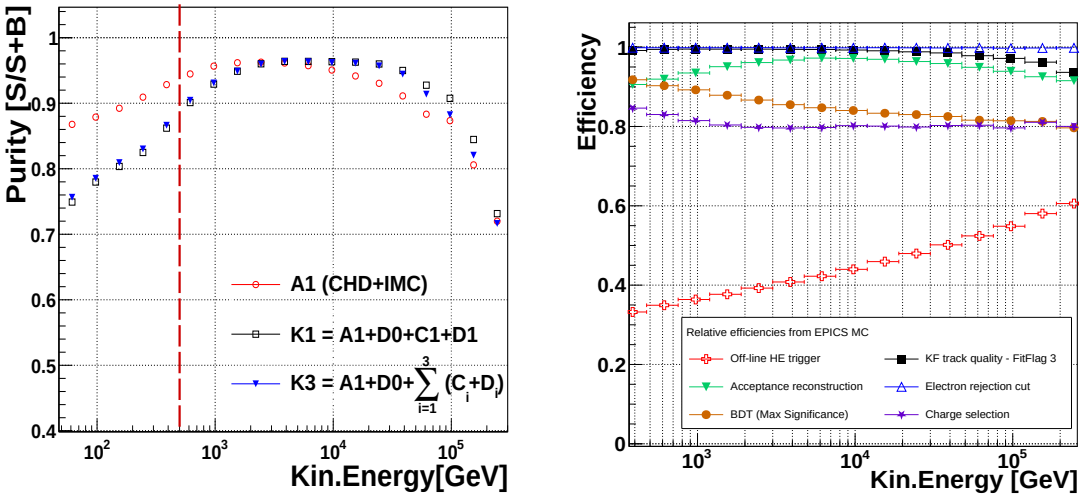

Figure 5: (Left) Purity quantity as function of kinetic energy for acceptance $\mathbf{A_1}$ with standard selections, and $\mathbf{K_1}$,$\mathbf{K_3}$ with BDT-based off-acceptance cuts. The red dashed line is set at 500 GeV kinetic energy. (Right) Efficiencies of $\mathbf{K_3}$ configuration for each selection step as function of kinetic energy.

4.2 Efficiencies and effective acceptance

For each selection stage, efficiency was calculated as the ratio of events passing the current stage to those passing all the previous ones. The results, for $\mathbf{K_3}$ configuration, are illustrated in the right-hand panel of Fig. 5. The results are compatible with the ones in fiducial acceptance for kinetic energies greater than 500 GeV. The effective acceptance[4] for configuration $\mathbf{A_1}$,$\mathbf{K_1}$ and $\mathbf{K_3}$ are shown in Fig. 6. A statistical gain up to $\sim$ 60% is achieved for $\mathbf{K_3}$ configuration with respect to $\mathbf{A_1}$.

[3]Background assessment has been performed with the same procedure of A_1 analysis [3].

[4]Defined as the total efficiency multiplied by the geometric factor.

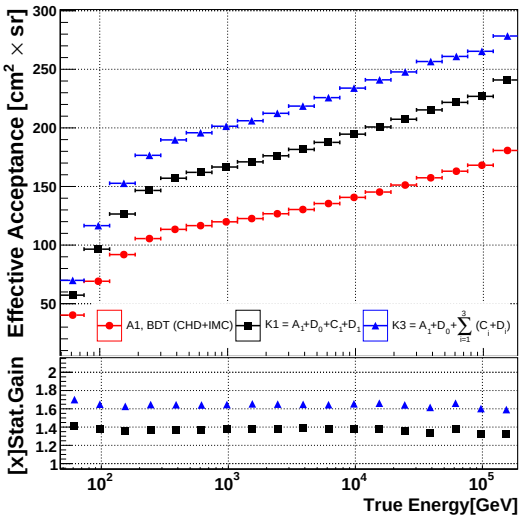

Figure 6: Effective acceptance for $\mathbf{A_1}$, $\mathbf{K_1}$ and $\mathbf{K_3}$, after applying the same type of selections to all, and, in the lower panel, the statistical gain for $\mathbf{K_1}$ and $\mathbf{K_3}$, is computed as $\frac{dN}{dE}$ after unfolding, normalized to $\mathbf{A_1}$ one.

4.3 Stability test of unfolding procedure

Extending the geometric acceptance to tracks with high tilt angles could impact the energy resolution for hadronic showers and therefore the unfolding procedure. Another key test to assess the feasibility of this extension is to verify the stability of the Bayesian unfolding procedure[5] for inferring the primary energy of the incoming particle from the fraction of energy deposited in the TASC [2]. The "pull test" has been selected for such validation.

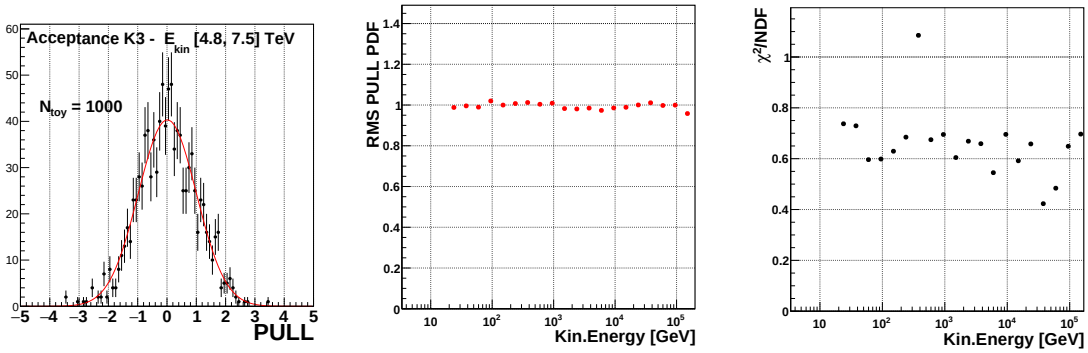

Figure 7: (Right) Pull distribution for energy bin E_{kin} : $4.8-7.5$ TeV obtained with $N_{toy} = 10^3$ simulations. (Middle) RMS and (Right) χ^2/NDF for Gaussian fit of pull distribution for each energy bin of the spectrum.

Each helium MC event from the acceptance K_3, which satisfies all the selection criteria, is fluctuated according to the Poisson distribution with a mean of one. This procedure is repeated N_{toy} times, resulting in $\{n_{DEP}^{TOY,i}\}_{i=1,\cdots,N_{toy}}$ newly sampled histograms[6] as a function of the deposited

[5]Performed with `ROOUnfold` package [6], using two iterations due to the accuracy of the prior distribution.

[6]Here n_{DEP} stands for $\frac{\mathrm{dN}}{\mathrm{dE_{DEP}}}$.

energy. Each of these histograms is then unfolded with the response matrix derived from no fluctuations in the MC sample, getting $\{n^{TOY,i}_{UNFLD}\}_{i=1,\cdots,N_{toy}}$. The pull distribution is then computed bin-by-bin as the difference between $n^{TOY,i}_{UNFLD}$ spectrum and the unfolded histogram derived without re-sampling n^{0}_{UNFLD}, divided by the statistical uncertainty σ^{0}_{UNFLD} provided by the unfolding routine in the latter case (Fig. 7).

For each energy bin, the pull distribution shows that the iterative Bayesian unfolding procedure from EPICS MC in $\mathbf{K_3}$ geometric configuration, is stable because the distributions from the pseudo-experiments can be fitted with a Gaussian curve to very high degree of accuracy (χ^2/NDF $\sim$ 1). The statistical uncertainties are estimated properly as well, since the RMS $\sim$ 1 in the entire energy range.

5. Conclusions

In our current helium analysis [3], approximately 50% of the total geometric factor is used to obtain the flux. Less stringent geometric requirements, using the same selections, lead to both a progressive increase in off-acceptance events and an overall rise in proton contamination. The former is mainly caused by the partial degradation of tracking performance for very inclined primaries, and the latter by the lack of the CHD sub-system for charge identification.

In this work, the possibility of mitigating these issues has been investigated by introducing a BDT-based off-acceptance background rejection, and an energy-dependent charge selection, both tailored to the topology of the event in extended acceptance.

The results indicate that extending the helium flux measurement to the K_3 acceptance is feasible above 500 GeV in kinetic energy, with a statistical gain up to $\sim$ 60%.

Acknowledgements We gratefully acknowledge JAXA's contributions to the development of CALET and to the operations onboard the International Space Station. The CALET effort in Italy is supported by ASI under Agreement No. 2013- 018-R.0 and its amendments. The CALET effort in the United States is supported by NASA through Grants No. 80NSSC20K0397, No. 80NSSC20K0399, and No. NNH18ZDA001N-APRA18-0004. This work is supported in part by JSPS Grant-in- Aid for Scientific Research (S) Grant No. 19H05608 in Japan.

References

[1] P. Maestro and N. Mori (for the CALET Collab.), PoS (ICRC2017) 208 (2017).
[2] P. Brogi et al. , PoS (ICRC2021) 101 (2021)
[3] O. Adriani et al. (CALET Collab.), Phys. Rev. Lett. **130**, 171002 (2023).
[4] J. J. Gomez et al., Nucl. Instr. Meth. Phys. Res. A, 262(2-3), 284–290, 1987.
[5] A. Hoecker, et al. "TMVA: Toolkit for Multivariate Data Analysis," PoS A CAT 040 (2007) [physics/0703039].
[6] L. Brenner,et al., Comparison of unfolding methods using RooFitUnfold, Int. J. Mod. Phys. A 35 (2020) 24, 2050145, arXiv:1910.14654 [physics.data-an].
[7] K. Kasahara, Proc. 24th Intl. Cosmic Ray Conf., Rome, Italy, ed. by N. Iucci and E. Lamanna (Intl. Union of Pure and Applied Phys. 1, 399 (1995)

Full Author List: CALET Collaboration

O. Adriani[1,2], Y. Akaike[3,4], K. Asano[5], Y. Asaoka[5], E. Berti[2,6], G. Bigongiari[7,8], W.R. Binns[9], M. Bongi[1,2], P. Brogi[7,8], A. Bruno[10], N. Cannady[11,12,13], G. Castellini[6], C. Checchia[7,8], M.L. Cherry[14], G. Collazuol[15,16], G.A. de Nolfo[10], K. Ebisawa[17], A.W. Ficklin[14], H. Fuke[17], S. Gonzi[1,2,6], T.G. Guzik[14], T. Hams[11], K. Hibino[18], M. Ichimura[19], K. Ioka[20], W. Ishizaki[5], M.H. Israel[9], K. Kasahara[21], J. Kataoka[22], R. Kataoka[23], Y. Katayose[24], C. Kato[25], N. Kawanaka[20], Y. Kawakubo[14], K. Kobayashi[3,4], K. Kohri[26], H.S. Krawczynski[9], J.F. Krizmanic[12], P. Maestro[7,8], P.S. Marrocchesi[7,8], A.M. Messineo[8,27], J.W. Mitchell[12], S. Miyake[28], A.A. Moiseev[29,12,13], M. Mori[30], N. Mori[2], H.M. Motz[31], K. Munakata[25], S. Nakahira[17], J. Nishimura[17], S. Okuno[18], J.F. Ormes[32], S. Ozawa[33], L. Pacini[2,6], P. Papini[2], B.F. Rauch[9], S.B. Ricciarini[2,6], K. Sakai[11,12,13], T. Sakamoto[34], M. Sasaki[29,12,13], Y. Shimizu[18], A. Shiomi[35], P. Spillantini[1], F. Stolzi[7,8], S. Sugita[34], A. Sulaj[7,8], M. Takita[5], T. Tamura[18], T. Terasawa[5], S. Torii[3], Y. Tsunesada[36,37], Y. Uchihori[38], E. Vannuccini[2], J.P. Wefel[14], K. Yamaoka[39], S. Yanagita[40], A. Yoshida[34], K. Yoshida[21], and W.V. Zober[9]

[1]Department of Physics, University of Florence, Via Sansone, 1 - 50019, Sesto Fiorentino, Italy, [2]INFN Sezione di Firenze, Via Sansone, 1 - 50019, Sesto Fiorentino, Italy, [3]Waseda Research Institute for Science and Engineering, Waseda University, 17 Kikuicho, Shinjuku, Tokyo 162-0044, Japan, [4]JEM Utilization Center, Human Spaceflight Technology Directorate, Japan Aerospace Exploration Agency, 2-1-1 Sengen, Tsukuba, Ibaraki 305-8505, Japan, [5]Institute for Cosmic Ray Research, The University of Tokyo, 5-1-5 Kashiwa-no-Ha, Kashiwa, Chiba 277-8582, Japan, [6]Institute of Applied Physics (IFAC), National Research Council (CNR), Via Madonna del Piano, 10, 50019, Sesto Fiorentino, Italy, [7]Department of Physical Sciences, Earth and Environment, University of Siena, via Roma 56, 53100 Siena, Italy, [8]INFN Sezione di Pisa, Polo Fibonacci, Largo B. Pontecorvo, 3 - 56127 Pisa, Italy, [9]Department of Physics and McDonnell Center for the Space Sciences, Washington University, One Brookings Drive, St. Louis, Missouri 63130-4899, USA, [10]Heliospheric Physics Laboratory, NASA/GSFC, Greenbelt, Maryland 20771, USA, [11]Center for Space Sciences and Technology, University of Maryland, Baltimore County, 1000 Hilltop Circle, Baltimore, Maryland 21250, USA, [12]Astroparticle Physics Laboratory, NASA/GSFC, Greenbelt, Maryland 20771, USA, [13]Center for Research and Exploration in Space Sciences and Technology, NASA/GSFC, Greenbelt, Maryland 20771, USA, [14]Department of Physics and Astronomy, Louisiana State University, 202 Nicholson Hall, Baton Rouge, Louisiana 70803, USA, [15]Department of Physics and Astronomy, University of Padova, Via Marzolo, 8, 35131 Padova, Italy, [16]INFN Sezione di Padova, Via Marzolo, 8, 35131 Padova, Italy, [17]Institute of Space and Astronautical Science, Japan Aerospace Exploration Agency, 3-1-1 Yoshinodai, Chuo, Sagamihara, Kanagawa 252-5210, Japan, [18]Kanagawa University, 3-27-1 Rokkakubashi, Kanagawa, Yokohama, Kanagawa 221-8686, Japan, [19]Faculty of Science and Technology, Graduate School of Science and Technology, Hirosaki University, 3, Bunkyo, Hirosaki, Aomori 036-8561, Japan, [20]Yukawa Institute for Theoretical Physics, Kyoto University, Kitashirakawa Oiwake-cho, Sakyo-ku, Kyoto, 606-8502, Japan, [21]Department of Electronic Information Systems, Shibaura Institute of Technology, 307 Fukasaku, Minuma, Saitama 337-8570, Japan, [22]School of Advanced Science and Engineering, Waseda University, 3-4-1 Okubo, Shinjuku, Tokyo 169-8555, Japan, [23]National Institute of Polar Research, 10-3, Midori-cho, Tachikawa, Tokyo 190-8518, Japan, [24]Faculty of Engineering, Division of Intelligent Systems Engineering, Yokohama National University, 79-5 Tokiwadai, Hodogaya, Yokohama 240-8501, Japan, [25]Faculty of Science, Shinshu University, 3-1-1 Asahi, Matsumoto, Nagano 390-8621, Japan, [26]Institute of Particle and Nuclear Studies, High Energy Accelerator Research Organization, 1-1 Oho, Tsukuba, Ibaraki, 305-0801, Japan, [27]University of Pisa, Polo Fibonacci, Largo B. Pontecorvo, 3 - 56127 Pisa, Italy, [28]Department of Electrical and Electronic Systems Engineering, National Institute of Technology (KOSEN), Ibaraki College, 866 Nakane, Hitachinaka, Ibaraki 312-8508, Japan, [29]Department of Astronomy, University of Maryland, College Park, Maryland 20742, USA, [30]Department of Physical Sciences, College of Science and Engineering, Ritsumeikan University, Shiga 525-8577, Japan, [31]Faculty of Science and Engineering, Global Center for Science and Engineering, Waseda University, 3-4-1 Okubo, Shinjuku, Tokyo 169-8555, Japan, [32]Department of Physics and Astronomy, University of Denver, Physics Building, Room 211, 2112 East Wesley Avenue, Denver, Colorado 80208-6900, USA, [33]Quantum ICT Advanced Development Center, National Institute of Information and Communications Technology, 4-2-1 Nukui-Kitamachi, Koganei, Tokyo 184-8795, Japan, [34]College of Science and Engineering, Department of Physics and Mathematics, Aoyama Gakuin University, 5-10-1 Fuchinobe, Chuo, Sagamihara, Kanagawa 252-5258, Japan, [35]College of Industrial Technology, Nihon University, 1-2-1 Izumi, Narashino, Chiba 275-8575, Japan, [36]Graduate School of Science, Osaka Metropolitan University, Sugimoto, Sumiyoshi, Osaka 558-8585, Japan, [37]Nambu Yoichiro Institute for Theoretical and Experimental Physics, Osaka Metropolitan University, Sugimoto, Sumiyoshi, Osaka 558-8585, Japan, [38]National Institutes for Quantum and Radiation Science and Technology, 4-9-1 Anagawa, Inage, Chiba 263-8555, Japan, [39]Nagoya University, Furo, Chikusa, Nagoya 464-8601, Japan, [40]College of Science, Ibaraki University, 2-1-1 Bunkyo, Mito, Ibaraki 310-8512, Japan

PoS(ICRC2023)082